Available online at www.sciencedirect.com

SciVerse ScienceDirect

Ceramics International 39 (2013) 1249–1255

CERAMICS INTERNATIONAL

www.elsevier.com/locate/ceramint

Electrical characterization of multidoped ceria ceramics

M. Stojmenović[a], S. Bošković[a], D. Bučevac[a,*], M. Prekajski[a], B. Babić[a], B. Matović[a], S. Mentus[b]

[a]*Institute of Nuclear Sciences "Vinča", Belgrade University, PO Box 522, 11 000 Belgrade, Serbia*
[b]*Faculty of Physical Chemistry, Belgrade University, Studentski trg 12, 11158 Belgrade, Serbia*

Received 12 June 2012; received in revised form 16 July 2012; accepted 17 July 2012
Available online 24 July 2012

Abstract

Ceria ceramics was obtained from multi-doped nanosized ceria powders prepared by both modified glycine nitrate procedure (MGNP) and self-propagating reaction at room temperature (SPRT). Rare earth elements such as Nd, Sm, Gd, Dy, Y, Yb were used as dopants. The overall mole fraction of dopants was 0.2. One-hour long sintering of powder compacts was performed at 1500 °C in oxygen atmosphere. Phase composition, microstructure and ionic conductivity of sintered samples were analysed. Single-phase ceria was detected in all samples. In general, the increase in the number of dopants improved the ionic conductivity. The samples doped simultaneously with five dopants had the highest ionic conductivity, as evidenced by the impedance measurements. At 450 °C, the conductivity of sample obtained by MGNP was $3.94 \times 10^{-3}\,\Omega^{-1}\,cm^{-1}$ whereas the conductivity of sample obtained by SPRT was $2.61 \times 10^{-3}\,\Omega^{-1}\,cm^{-1}$. The conductivity activation energy for MGNP and SPRT samples was measured to be 0.348 and 0.385 eV, respectively. Finally, the conductivity decreased as the number of dopants increased to six.

Keywords: A. Sintering; C. Ionic conductivity; D. CeO_2; E. Fuel cells

1. Introduction

Ceria (CeO_2) is promising electrolyte material for intermediate temperature solid oxide fuel cells (SOFCs) thanks to its high electrical (ionic) conductivity. The fluorite type crystal structure of ceria allows accommodation of relatively large amount of rare earth cations which can affect ionic conductivity of ceria [1]. It is well documented that the substitution of trivalent cation for Ce^{4+} cation introduces oxygen vacancies as a result of charge compensation [2]. The vacancies enable the mobility of oxygen anions, i.e., the transport of oxygen from cathode to anode in SOFCs. Besides the increase in vacancy concentration, the doping by aliovalent cations creates an inevitable distortion of ceria lattice due to the difference in ionic radii of the dopant ions and Ce^{4+} ion. The lattice distortion, which is also expected to affect conductivity, can be controlled by a simultaneous doping with different cations. Several authors have reported that the electrical conductivity of multidoped material can be even 30% higher than that of single doped material [3].

Although a clear relationship between grain size and conductivity of a solid electrolyte has not been established yet, some authors have reported that the reduction in grain size of electrolyte helped to improve its conductivity [4]. Thus, it is essential to fabricate fine, nanosized, starting powders with high specific surface area and therefore high driving force for sintering which allows densification at temperature lower than that required for micron sized powders. The advantage of the use of nanosized starting powders is not only the reduction in production cost but also the reduction in grain size of sintered samples.

In our previous study, various multidoped ceria nanopowders were synthesized by both MGNP and SPRT method, and a comparative analysis of their physicochemical properties was performed [5]. It was shown that the difference in composition of ceria powders caused the differences in specific surface area, crystallite size, microstrain value and porosity type.

*Corresponding author. Tel.: +381 11 340 8723; fax: +381 11 340 8224.
E-mail address: bucevac@vinca.rs (D. Bučevac).

0272-8842/$ - see front matter © 2012 Elsevier Ltd and Techna Group S.r.l. All rights reserved.
http://dx.doi.org/10.1016/j.ceramint.2012.07.055

The subject of the present study is ionic conductivity of sintered multidoped ceria samples and its correlation to the density and microstructure. Even six dopants were added simultaneously. According to authors' knowledge, the study of ionic conductivity of ceria doped with such a large number of dopants has not been published so far.

2. Material and methods

Experimental work was focused on sintering of ceria nanopowders containing from one to six dopants. The overall mole fraction of dopants was 0.2. Powders with following compositions were used:

1. CeO_2,
2. $Ce_{0.8}Gd_{0.20}O_{2-\delta}$,
3. $Ce_{0.8}Sm_{0.08}Gd_{0.12}O_{2-\delta}$,
4. $Ce_{0.8}Sm_{0.01}Gd_{0.01}Y_{0.18}O_{2-\delta}$,
5. $Ce_{0.8}Sm_{0.005}Gd_{0.005}Dy_{0.095}Y_{0.095}O_{2-\delta}$,
6. $Ce_{0.8}Nd_{0.01}Sm_{0.04}Gd_{0.04}Dy_{0.04}Y_{0.07}O_{2-\delta}$,
7. $Ce_{0.8}Nd_{0.01}Sm_{0.015}Gd_{0.025}Dy_{0.04}Y_{0.05}Yb_{0.06}O_{2-\delta}$.

Two different methods were employed to fabricate the above mentioned powders. Although the detail procedure was given elsewhere [5] it would be quite useful to briefly compare these two techniques.

The first one is so-called modified glycine nitrate procedure (MGNP) which proceeds according to the following reaction [6]:

$$4NH_2CH_2COOH + 2[(1-x)Ce(NO_3)_3 \cdot 6H_2O + xMe(NO_3)_3 \cdot 6H_2O] + 2O_2 \rightarrow 2Ce_{1-x}Me_xO_{2-\delta} + 22H_2O\uparrow + 5N_2\uparrow + 8CO_2\uparrow$$

where Me is Nd, Sm, Gd, Dy, Y, Yb and x is the overall mole fraction of dopants. Glycine (NH_2CH_2COOH) and nitrate hexahydrates of dopant ions were dissolved in distilled water and heated up to 450 °C until the evaporation stopped. The obtained ashes were calcined at 600 °C to burn up the organic remains.

The second technique is self-propagating reaction at room temperature (SPRT) which is based on the mechanically activated reaction between cerium nitrate, nitrates of dopant ions and sodium hydroxide, as described by the following equation [7]:

$$2[(1-x)Ce(NO_3)_3 \cdot 6H_2O + xMe(NO_3)_3 \cdot 6H_2O] + 6 \cdot NaOH + (1/2-\delta)O_2 \rightarrow 2Ce_{1-x}Me_xO_{2-\delta} + 6NaNO_3 + 15H_2O \quad (2)$$

The advantage of this method is the possibility of obtaining nanopowders by hand mixing at room temperature without additional calcination.

The synthesized powders were pressed into pellets under uniaxial pressure of 50 MPa, followed by cold isostatic pressing at 225 MPa. The pellets were sintered in a horizontal furnace at 1500 °C for 1 h in oxygen atmosphere. Heating rate was 5 °C/min. Diameter of the sintered samples was about 5 mm whereas the thickness was about 3 mm. The density of sintered samples was determined by Archimedes' method.

The scanning electron microscopy (SEM) analysis was performed using a JEOL 6300 F microscope at a 3 kV accelerating voltage. Surfaces of the sintered samples were polished and then thermally etched in order to reveal the grain boundaries. Crystalline phases were identified by X-ray diffraction (XRD) using filtered Cu-K_α radiation (Siemens D5000). The structural refinement was performed with the FullProf computer program [8–10] which adopts the Rietveld calculation method for the samples with five dopants.

The electrical properties were measured by electrochemical impedance method, in the frequency range 1 Hz–0.1 MHz, using Gamry 750 ZRA potentiostat/galvanostat and EIS300 Impedance Software. The measurements were conducted in air, in the temperature range 200–450 °C, with 50 °C increment. The amplitude of the applied sinusoidal voltage signal was 50 mV. Thin layer of high conductivity silver paste was applied onto both sides of the sample pellets in order to provide good electrical contact between electrolyte and electrodes. The samples were placed between the silver plates in a quartz holder which was heated by vertical oven. A Pt–Rh thermocouple located just below the bottom silver plate was used for temperature monitoring. The impedance data were used to estimate appropriate equivalent circuit by means of the software Z-View2 (version 2.6 demo).

The resistance values were determined from the impedance diagrams recorded at various temperatures. The specific conductance was calculated from the resistance data using the dimensions of the sample pellets.

3. Results and discussion

It will be shown later that the highest electrical conductivity was measured in ceria samples containing five dopants. Therefore the samples with composition $Ce_{0.8}Nd_{0.01}Sm_{0.04}Gd_{0.04}Dy_{0.04}Y_{0.07}O_{2-\delta}$ synthesised by the two different methods will be thoroughly discussed in the following sections.

3.1. Structure details of powders and sintered samples

As Fig. 1 shows, the synthesised powders as well as sintered samples with five dopants exhibit a single phase composition despite high concentration of dopants. In order to confirm the phase composition, Rietveld refinement was performed for the powders containing five dopants and corresponding sintered pellets. The data reported by Kuemmerle and Heger [11] were used as the starting structural model for the refinement. Important structural parameters such as lattice parameter (a), Ce–O bond length (Ce–O), crystallite size (D), microstrain (e) as well as corresponding agreement factors R_{wp} and C_h^2 are presented in Table 1. The reasonable values of corresponding agreement factors indicate a

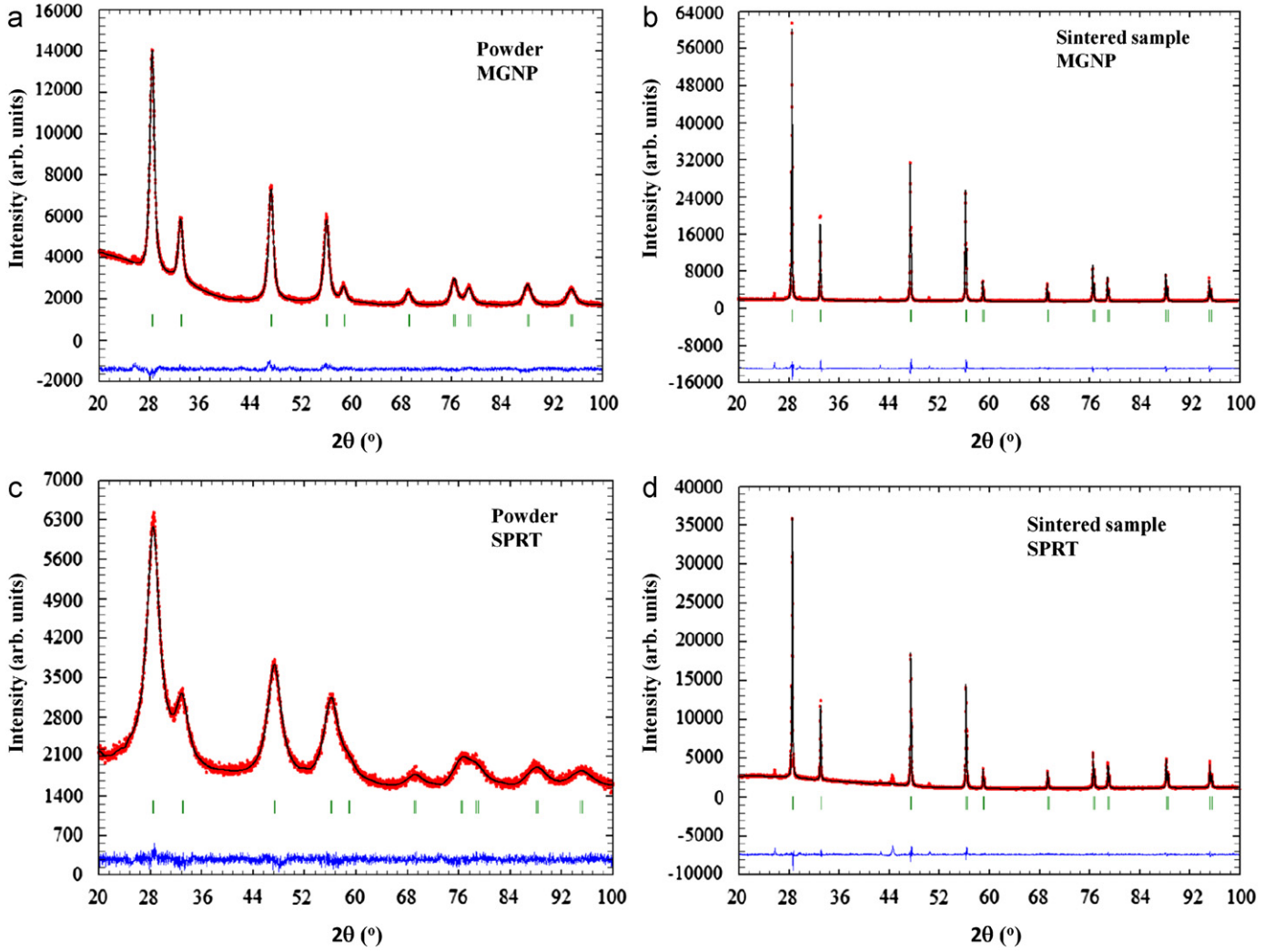

Fig. 1. XRD structural refinement patterns of powders and corresponding sintered samples containing five dopants (No 6) prepared by: (a), (b) MGNP and (c), (d) SPRT method. A difference plot which shows the difference between recorded pattern and pattern obtained by Rietveld's method is shown beneath. Tick marks above the difference data indicate the reflection positions.

Table 1
Lattice parameter (a), Ce–O bond length (Ce–O), crystallite size (D), microstrain (e) and corresponding agreement factors (R_{wp}) and (C_h^2) of ceria nanopowders and sintered ceramics with five dopants (No 6) obtained by MGNP and SPRT methods.

Sample composition ($Ce_{0.8}Nd_{0.01}Sm_{0.04}Gd_{0.04}Dy_{0.04}Y_{0.07}\ O_{2-\delta}$)	a (Å)	Ce–O (Å)	D (nm)	$e \times 10^3$ (Å)	R_{wp}	C_h^2
Powder synthesized by MNGP	5.43215(2)	2.352193(4)	16	82	9.18	1.55
Powder synthesized by SPRT	5.43249(6)	2.352337(1)	2	157	7.91	1.13
Sintered sample MNGP	5.42439(9)	2.348833(8)	–	–	10.90	3.82
Sintered sample SPRT	5.42022(8)	2.347027(5)	–	–	13.30	3.43

successful refinement. As Table 1 indicates, the lattice parameter, a, as well as the length of Ce–O bond are almost constant for all samples. Furthermore, it is important to note that the crystallite size of powder obtained by MGNP method is considerably larger than that of the powder obtained by SPRT. It is believed that the larger crystallite size of MGNP powder is a result of 4-h long calcination at 600 °C which was employed to burn up the organic remains in MGNP powder. Unlike MGNP powder, SPRT powder was not calcinated as simple rinsing in distilled water and alcohol was sufficient to remove by-products such as $NaNO_3$. The calcination is also considered to be the reason for stress relaxation in MGNP powder crystals. As Table 1 evidences, the microstrain in MGNP samples is considerably lower than that of SPRT samples. In addition, the values for crystallite size of sintered samples are not given in Table 1 as it was very difficult to

determine the actual area of sharp XRD peaks of these samples and therefore to calculate the crystallite size.

Although the thorough analysis of particle size of obtained powders was conducted in the previous study [5] it would be important to mention again that the average particle size of MGNP and SPRT powders with five dopants was 15 and 3.17 nm. Particle size distribution was not actually plotted as the size distribution was fairly narrow. For example, particle size of MGNP powder varied from 13 to 18 nm whereas the particle size of SPRT varied from 2 to 5 nm. Nevertheless, these results show good agreement with crystallite size values given in Table 1.

3.2. Densification and microstructure

The density of sintered samples is presented in Table 2. The samples synthesized by MGNP method achieved higher density (90–95%TD) than the samples obtained by SPRT method (83–90%TD). This finding is quite unexpected since the crystallite size of SPRT powders (2 nm) is smaller than that of MGNP powders (16 nm) and therefore driving force for sintering of SPRT powders, i.e., density is expected to be higher than that of MGNP powders. It is believed that the pronounced agglomeration of very fine SPRT powders is the main reason for relatively low sintered density of these samples. Very small pores in agglomerates lead to less compact particle packing of SPRT samples and therefore lower final sintered density than that of MGNP samples. This conclusion is supported by the detailed morphological analysis of synthesised powders conducted in the previous study [5]. As Table 2 indicates, the number of dopants shows strong influence on the final sintered density. Maximum density was measured for triple doped ceramics obtained from both MGNP and SPRT powders. Further increase in the number of dopants is accompanied by a decrease in the final sintered density.

Microstructures of triple doped sintered samples obtained from MGNP to SPRT powders are presented in Fig. 2. It is evident that the powder synthesis technique strongly affects not only the sintered density but also the size and morphology of grains. Smaller grains, narrow grain size distribution and higher porosity are characteristic for sintered samples obtained from SPRT powder. On the other side, the samples obtained from MGNP powder

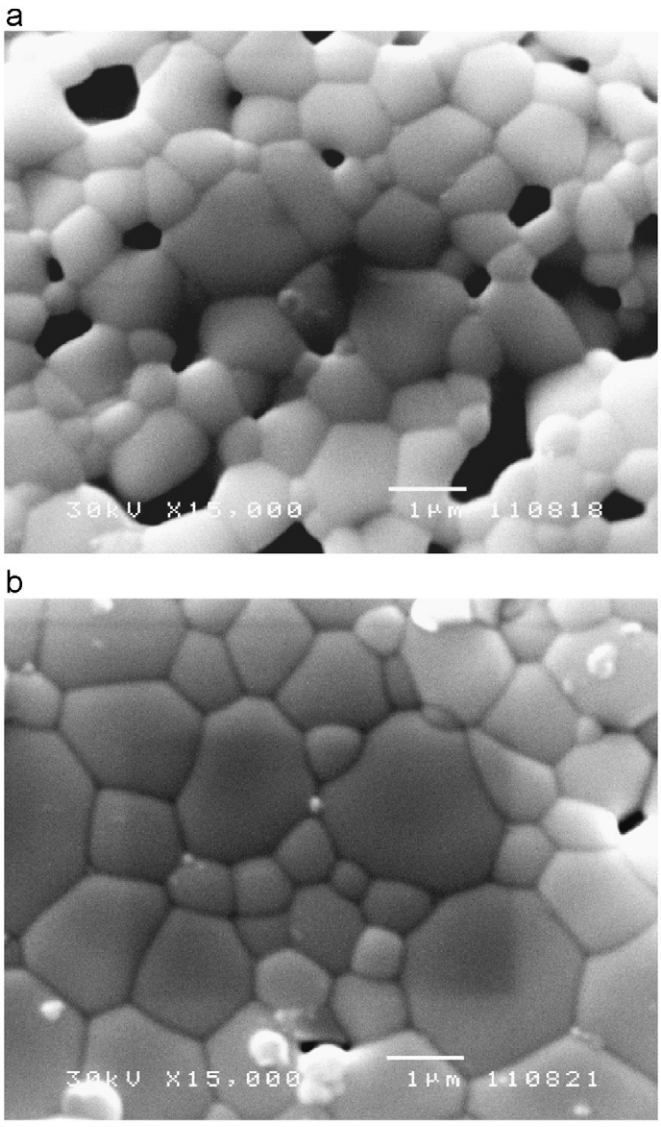

Fig. 2. SEM micrographs of triple doped ceria samples (No 4), sintered at 1500 °C for 1 h, obtained by: (a) SPRT and (b) MGNP method.

Table 2
Density of samples obtained by sintering of MGNP and SPRT powder compacts at 1500 °C for 1 h.

Composition	Theoretical density ($g\,cm^{-3}$)	Powder synthesis route			
		MGNP		SPRT	
		Sintered density ($g\,cm^{-3}$)	Relative density (TD %)	Sintered density ($g\,cm^{-3}$)	Relative density (TD %)
1. CeO_2	7.21	6.65	92.26	6.34	87.96
2. $Ce_{0.8}Gd_{0.20}O_{2-\delta}$,	7.23	6.84	94.66	6.24	86.35
3. $Ce_{0.8}Sm_{0.08}Gd_{0.12}O_{2-\delta}$,	7.18	6.77	94.22	6.43	89.49
4. $Ce_{0.8}Sm_{0.01}Gd_{0.01}Y_{0.18}O_{2-\delta}$,	6.77	6.44	95.11	5.98	90.21
5. $Ce_{0.8}Sm_{0.005}Gd_{0.005}Dy_{0.095}Y_{0.095}O_{2-\delta}$	7.61	7.17	94.25	6.37	88.32
6. $Ce_{0.8}Nd_{0.01}Sm_{0.04}Gd_{0.04}Dy_{0.04}Y_{0.07}O_{2-\delta}$	7.03	6.34	91.07	6.39	88.08
7.$Ce_{0.8}Nd_{0.01}Sm_{0.015}Gd_{0.025}Dy_{0.04}Y_{0.05}Yb_{0.06}O_{2-\delta}$	7.18	6.54	90.92	6.26	83.17

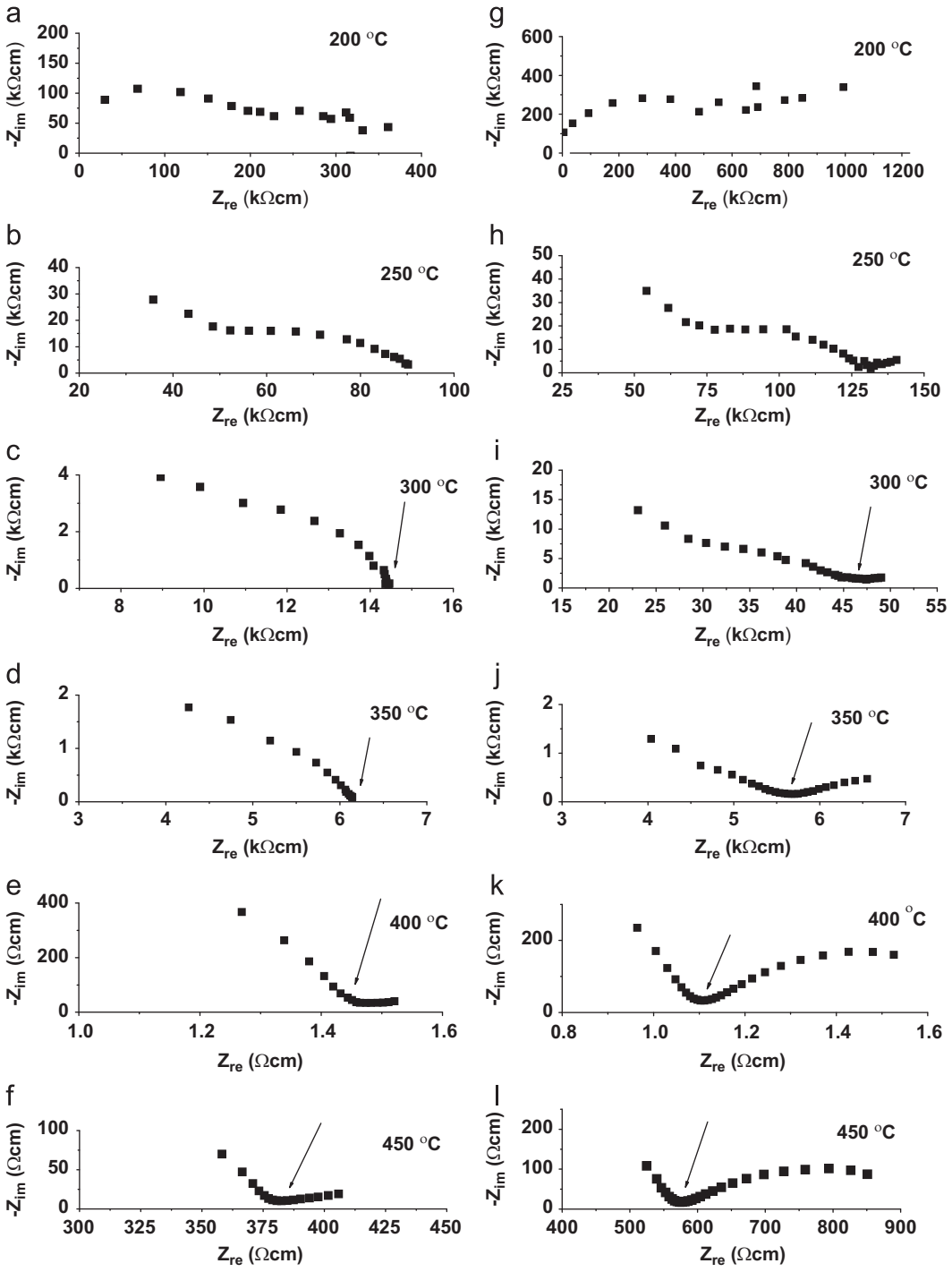

Fig. 3. Impedance diagrams of sintered samples containing five dopants (No 6), synthesized by MGNP (left column) and SPRT (right column) methods measured at different temperture. The frequency increases from right to left. The arrows indicate the points on the real axis which correspond to the R_b+R_{gb}.

possess larger grains, bimodal grain size distribution and less pronounced porosity.

3.3. Electrical conductivity

Fig. 3 shows original Nyquist's diagrams of the samples containing five dopants (No 6) obtained by both MGNP and SPRT method. These samples were chosen as they have the highest conductivity. The diagrams were recorded within the temperature range 200–450 °C, with an increment of 50 °C. As Fig. 3 reveals, two adjacent, remarkably distorted, impedance semicircles were observed in the available frequency range, 1 Hz–0.1 MHz, at 200 and 250 °C. Such a type of Nyquist plot is characteristic of a two serially connected RC circuits, both of which containing one resistive and one capacitive element bonded in

a parallel arrangement. The capacitive element is frequency dependent (distributed) one. Such an equivalent circuit with both constant [12–14] and distributed [15] element was applied widely in the literature related to the sintered ceramics. The high-frequency semicircle may be attributed to a parallel connection of the bulk resistance (R_b) of crystalline grains and the geometric capacitance (C_g) of the sample. The low-frequency semicircle may be attributed to a parallel connection of the grain boundary resistance (R_{gb}) and the intergranular capacitance (C_{ig}). If the impedance semicircles are clearly separated, i.e., $R_bC_g << R_{gb}C_{ig}$, the values of R_b and R_{gb} can be read separately as a low-frequency intercepts of the semicircles with the real axis. By means of the frequency corresponding to the high-frequency semicircle maximum, $\omega_{max,b}$, geometric capacitance (C_g) can be calculated according to the following equation:

$$\omega_{max,b} = 1/R_b \times C_g \quad (3)$$

In the case of the low-frequency semicircle the intergranular capacitance (C_{ig}) can be calculated using the following equation:

$$\omega_{max,gb} = 1/R_{gb} \times C_{ig} \quad (4)$$

As Fig. 3 shows, both R_b and R_{gb} decrease as the temperature increases. According to Eq. (3) and Eq. (4), the decrease in R_b and R_{gb} causes an increase in $\omega_{max,b}$ and $\omega_{max,gb}$ which results in shifting of whole region of the impedance points towards the low-frequency semicircle. Therefore, R_b and R_{gb} cannot be distinguished at high temperatures such as 300 °C (Fig. 3c and i). In the available frequency range, only the sum of R_b and R_{gb} (R_b+R_{gb}) can be determined from real axis intercept as indicated by arrows in diagrams given in Fig. 3.

New semicircle, which is particularly visible for SPRT sample, appears in the low-frequency region at temperatures 400 and 450 °C (Fig. 3e, f, k, and l). It is believed that this semicircle is associated with formation of oxygen ions at the electrode-sample interface through reaction: $O_2+4e^- \rightarrow 2O^{2-}$. However, this reaction does not belong to the scope of this study.

The total resistance values measured for all samples were used to calculate specific conductivity at different temperatures. The obtained values of ionic conductivity of sintered samples synthesized by MGNP and SPRT method are listed in Tables 3 and 4. By comparing the results obtained for the two groups of samples, it can be seen that samples having five dopants (Nd^{3+}, Sm^{3+}, Gd^{3+}, Dy^{3+}, Y^{3+}), assigned by No 6, obtained by both MGNP and SPRT method exhibit the highest values of ionic conductivity. The conductivity values measured at 450 °C are 3.94×10^{-3} and 2.61×10^{-3} Ω^{-1} cm^{-1} for MGNP and SPRT samples, respectively. It is interesting to note that the samples with six dopants, assigned by No 7, obtained by both MGNP and SPRT method have lower ionic conductivity than that of samples with six dopants. Therefore, it can be suggested that there is a possibility that some combination of the dopants involving *Yb* decreases ionic

Table 3
Ionic conductivity, κ, of the samples obtained by MGNP method measured at different temperatures.

No.	Composition (MGNP)	Temperature					
		200 °C κ (Ω^{-1} cm^{-1})	250 °C	300 °C	350 °C	400 °C	450 °C
1.	CeO_2	6.00×10^{-6}	2.17×10^{-5}	1.12×10^{-4}	2.10×10^{-4}	3.85×10^{-4}	6.12×10^{-4}
2.	$Ce_{0.8}Gd_{0.20}O_{2-\delta}$	6.67×10^{-6}	2.16×10^{-6}	1.42×10^{-4}	5.95×10^{-4}	1.50×10^{-3}	3.61×10^{-3}
3.	$Ce_{0.8}Sm_{0.08}Gd_{0.12}O_{2-\delta}$	2.73×10^{-6}	2.86×10^{-5}	1.67×10^{-4}	5.21×10^{-4}	1.50×10^{-3}	2.26×10^{-3}
4.	$Ce_{0.8}Sm_{0.01}Gd_{0.01}Y_{0.18}O_{2-\delta}$	1.46×10^{-5}	3.90×10^{-5}	1.58×10^{-5}	2.18×10^{-4}	2.76×10^{-4}	2.22×10^{-3}
5.	$Ce_{0.8}Sm_{0.005}Gd_{0.005}Dy_{0.095}Y_{0.095}O_{2-\delta}$	1.88×10^{-6}	5.73×10^{-6}	2.87×10^{-5}	1.66×10^{-4}	6.28×10^{-4}	2.04×10^{-3}
6.	$Ce_{0.8}Nd_{0.01}Sm_{0.04}Gd_{0.04}Dy_{0.04}Y_{0.07}O_{2-\delta}$	4.17×10^{-6}	1.67×10^{-5}	1.03×10^{-4}	2.44×10^{-4}	1.02×10^{-3}	3.94×10^{-3}
7.	$Ce_{0.8}Nd_{0.01}Sm_{0.015}Gd_{0.025}Dy_{0.04}Y_{0.05}Yb_{0.06}O_{2-\delta}$	3.17×10^{-6}	1.05×10^{-6}	7.58×10^{-5}	2.22×10^{-4}	4.01×10^{-4}	7.77×10^{-4}

Table 4
Ionic conductivity, κ, of the samples obtained by SPRT method measured at different temperatures.

No.	Composition (SPRT)	Temperature					
		200 °C κ ($\Omega^{-1}cm^{-1}$)	250 °C	300 °C	350 °C	400 °C	450 °C
1.	CeO_2	7.32×10^{-6}	3.07×10^{-5}	6.67×10^{-5}	5.56×10^{-4}	1.11×10^{-3}	1.90×10^{-3}
2.	$Ce_{0.8}Gd_{0.20}O_{2-\delta}$	6.67×10^{-6}	2.01×10^{-5}	9.55×10^{-5}	2.27×10^{-4}	9.20×10^{-4}	2.14×10^{-3}
3.	$Ce_{0.8}Sm_{0.08}Gd_{0.12}O_{2-\delta}$	3.66×10^{-6}	1.88×10^{-5}	4.62×10^{-5}	1.93×10^{-4}	9.38×10^{-4}	1.82×10^{-3}
4.	$Ce_{0.8}Sm_{0.01}Gd_{0.01}Y_{0.18}O_{2-\delta}$	2.36×10^{-6}	3.16×10^{-5}	6.38×10^{-5}	5.45×10^{-4}	1.11×10^{-3}	1.88×10^{-3}
5.	$Ce_{0.8}Sm_{0.005}Gd_{0.005}Dy_{0.095}Y_{0.095}O_{2-\delta}$	7.32×10^{-6}	2.31×10^{-5}	5.77×10^{-5}	1.79×10^{-4}	5.45×10^{-4}	1.29×10^{-3}
6.	$Ce_{0.8}Nd_{0.01}Sm_{0.04}Gd_{0.04}Dy_{0.04}Y_{0.07}O_{2-\delta}$	1.88×10^{-6}	1.19×10^{-5}	3.18×10^{-5}	2.63×10^{-4}	1.35×10^{-3}	2.61×10^{-3}
7.	$Ce_{0.8}Nd_{0.01}Sm_{0.015}Gd_{0.025}Dy_{0.04}Y_{0.05}Yb_{0.06}O_{2-\delta}$	1.58×10^{-6}	1.15×10^{-5}	7.50×10^{-5}	3.75×10^{-4}	8.43×10^{-4}	1.59×10^{-3}

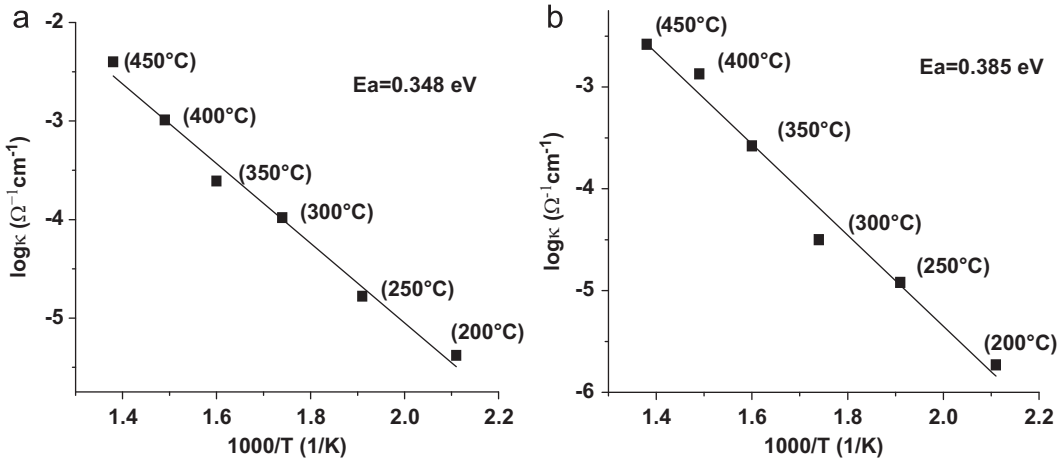

Fig. 4. The dependence $\log\kappa = f(1/T)$ for sintered samples containing five dopants (No. 6) obtained by (a) MGNP and (b) SPRT method.

mobility. Furthermore, the addition of six dopants changed the density of samples, which may be also responsible for the decrease in electrical conductivity.

Based on the results listed in Tables 3 and 4, the dependence $\log k = f(1/T)$ for samples with five dopants (No 6) obtained by both SPRT and MGNP method was plotted in Fig. 4. Again, these samples were chosen as they showed the highest conductivity. The activation energy of migration of oxide ions, Ea, was calculated based on the slope of plots given in Fig.4. It was found that the activation energy for MGNP and SPRT samples was 0.348 and 0.385 eV, respectively. Somewhat lower activation energy for MGNP sample confirms the rule that the activation energy decreases with the increase in density (decrease in porosity).

4. Conclusions

Single-phase, multi doped, ceria nanopowders were obtained by modified glycine nitrate procedure (MGNP) and self-propagating reaction at room temperature (SPRT). When it comes to the powders containing five dopants the larger crystallite size was measured for MGNP powder whereas the larger microstrain was measured for SPRT powder crystals. Higher density of sintered MGNP samples than that of SPRT samples was a result of better particle packing in green compacts made of MGNP powder. The highest ionic conductivity was measured at 450 °C in samples containing five dopants (No 6) obtained by both MGNP and SPRT method. Higher ionic conductivity of MGNP samples ($3.94 \times 10^{-3}\,\Omega^{-1}\,cm^{-1}$) than that of SPRT samples ($2.61 \times 10^{-3}\,\Omega^{-1}\,cm^{-1}$) was attributed to the higher density of MGNP samples. Further increase in the number of dopants to six (No 7) led to the decrease in ionic conductivity. It appears that the additional doping by Yb^{3+} inhibits the oxygen anion mobility.

Acknowledgements

This work has been supported by the Ministry of Education and Science of Serbia (project number: 45012).

References

[1] T. Mori, J. Drennan, J.H. Lee, J.G. Li, T. Ikegami, Oxide ionic conductivity and microstructures of Sm- or La-doped CeO_2-based systems, Solid State Ionics 154–155 (2002) 461–466.
[2] S. Tsunekawa, T. Fukuda, A. Kasuya, X-ray photoelectron spectroscopy of monodisperse CeO_{2-x} nanoparticles, Surface Science Letters 457 (2000) 437–440.
[3] S. Bošković, S. Zec, G. Branković, Z. Branković, A. Devečerski, B. Matović, F. Aldinger, Preparation, sintering and electrical properties of nano-grained multidoped ceria, Ceramics International 36 (2010) 121–127.
[4] J.P. Gonjal, R. Schmidt, J.E. Canuto, P.R. Alvarez, E. Moran, Increased ionic conductivity in microwave hydrothermally synthesized rare-earth doped ceria $Ce_{1-x}RE_xO_{2-(x/2)}$, Journal of Power Sources 209 (2012) 163–171.
[5] M. Stojmenović, S. Bošković, S. Zec, B. Babić, B. Matović, D. Bučevac, Z. Dohčević-Mitrović, F. Aldinger, Characterization of nanometric multidoped ceria powders, Journal of Alloys and Compounds 507 (2010) 279–285.
[6] S.B. Bošković, B.Z. Matović, M.D. Vlajić, V.D. Kristić, Modified glycine nitrate procedure (MGNP) for the synthesis of SOFC nanopowders, Ceramics International 33 (2007) 89–93.
[7] S. Bošković, D. Đurović, Z. Dohčević-Mitrović, Z. Popović, M. Zinkevich, A. Aldinger, Self-propagating room temperature synthesis of nanopowders for solid oxide fuel cells (SOFC), Journal of Power Sources 145 (2005) 237–242.
[8] Rodriguez-Carvajal J., FullProf computer program (1998), 〈ftp://charybde.saclay.cea.fr/pub/divers/fullprof.98/windows/winfp98.zip〉.
[9] J. Rodriguez-Carvajal, Recent advances in magnetic structure determination by neutron powder diffraction, Physica B 192 (1993) 55–69.
[10] J. Rodriguez-Carvajal, Recent developments of the program FULLPROF, Commission on Powder Diffraction (IUCr), Newsletter 26 (2001) 12–19.
[11] E.A. Kuemmerle, G. Heger, The structures of C-(Ce_2O_{3+d}), Ce_7O_{12} and $Ce_{11}O_{20}$, Journal of Solid State Chemistry 147 (1999) 485–500.
[12] R. Waster, R. Hagenbeck, Grain boundaries in dielectric and mixed-conducting ceramics, Acta Materialia 48 (2000) 797–825.
[13] X.J. Chen, K.A. Khor, S.H. Chan, L.G. Yu, Preparation yttria – stabilized zirconia electrolyte by spark – plasma sintering, Materials Science and Engineering A 341 (2003) 43–48.
[14] D. Pérez-Coll, P. Núñez, J.R. Frade, The role of SiO_2 and sintering temperature on the grain boundary properties of $Ce_{0.8}Sm_{0.2}O_{2-\delta}$, Journal of Power Sources 196 (2011) 8383–8390.
[15] M.R. Kosinski, R.T. Baker, Preparation and property – performance relationships in samarium – doped ceria nanopowders for solid oxide fuel cell electrolytes, Journal of Power Sources 196 (2011) 2498–2512.